

# Mechanical oscillations of an oxidizing agent over a mercury surface

Björn Maiworm and Mario Markus\*

Max-Planck-Institut für Molekulare Physiologie, Postfach 500247, D-44202 Dortmund, Germany.

\* Corresponding author, E-mail: markus@mpi-dortmund.mpg.de

Received 31 Mar 2005

Accepted 12 Jul 2005

**ABSTRACT:** A drop of a solution of potassium dichromate and sulphuric acid was placed on the surface of mercury around an iron needle immersed in the mercury. We observed circular, as well as irregularly swirling oscillations of this drop. We could explain this phenomenon as follows. Electrochemical oscillations occur at the iron-solution interface; these cause oscillations of the potential at the drop's bottom, and thus of the drop's shape by virtue of electrocapillarity. Our measurements allowed us to determine the surface tension and the capacity of the double-layer at the mercury-solution interface, as functions of voltage. We observed and explain a much faster electrical loading, as compared to the unloading, of the double-layer. Furthermore, we observed a negative differential electrical capacity.

**KEYWORDS:** surface tension, electrochemical oscillations, beating mercury heart, electrocapillarity.

## INTRODUCTION

The setup we present in this work is related to the setup of the well-known beating mercury heart<sup>1-5</sup>. The latter (Fig. 1a), consists of a mercury drop and an iron needle, both covered by an oxidizing solution *S*. The oxidation of the mercury causes the mercury's surface to become positively charged and thus its surface tension to decrease. This causes a flattening of the mercury drop, which allows contact of the mercury drop with the iron. The iron neutralizes the charge at the mercury's surface, so that the initial situation shown in the scheme in Fig. 1a is recovered; i.e. one beating cycle is completed.

The setup in this work is illustrated in Fig. 1b. A drop of the oxidizing solution is placed on a mercury-surface, while an iron needle is constantly in contact with both the mercury and the solution. A beating of the drop of solution is observed. As we will describe below, this phenomenon is mechanistically different to the beating mercury heart since the drop of solution is driven, in the present case, by electrochemical processes at the sustained iron-solution contact surface.

In this work we will first give details of the setup and will describe how to get self-oscillations started. We will then present the observations of the mechanical and of the electrical oscillations. Then, we will induce changes in the radius of the drop by applying voltage steps on the system. It will be shown that the increase of the radius, as the voltage drops, is much slower than the decrease of the radius as the voltage rises; this relaxation asymmetry is also observed for the self-

oscillations. Next, we will determine the surface tension of the mercury in contact with the solution, the charge of the mercury surface and the capacity of the mercury-solution double-layer, as functions of voltage (For information on electrical double-layers, see Ref. 6). Using our measurements, we will then explain the relaxation asymmetry.

## MATERIALS, METHODS AND MEASUREMENTS

A watch glass with diameter 15 cm was filled with mercury up to a central height of 13 mm. The oxidizing solution contained  $K_2Cr_2O_7$  (1.16 mM) and  $H_2SO_4$  (7 M). The surface tension of this solution (in contact with

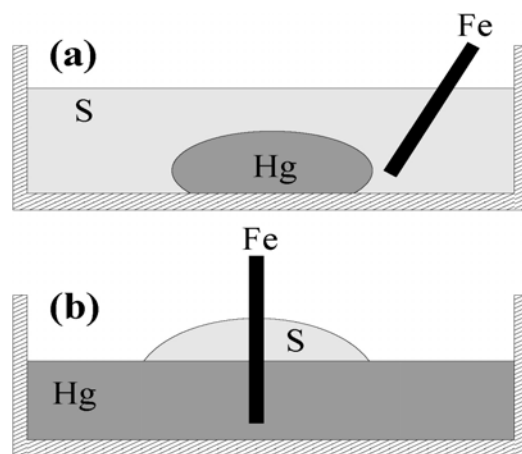
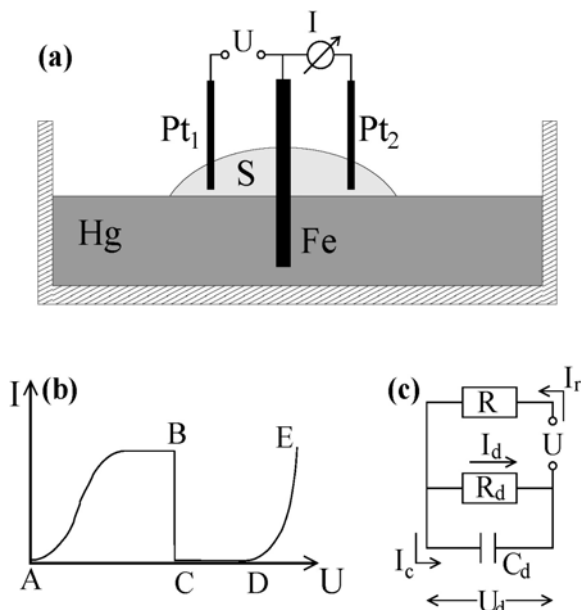


Fig 1. Schemes of the experimental setups for the beating mercury heart (a) and for the beating oxidizing solution drop described in this work (b). *S*: Oxidizing solution.

air), as measured with a capillary tube, is  $\sigma_{SA} = 70.5$  dyn/cm. A drop (volume  $D = 0.2$  ml) of this solution was poured around an iron needle (length: 40 mm; diameter: 1 mm), which had been placed vertically through the mercury at its center (see Fig. 1b). The shape of the drop self-organized symmetrically as a circle around this needle.

Fig. 2a shows a scheme of the setup we used to start oscillations. Fig. 2b shows schematically a typical current-voltage characteristic of a metal-electrolyte system<sup>7,8</sup>, such as that shown in Fig. 2a. Between the points A and B in Fig. 2b ("activity" regime), corrosion takes place, i.e. iron goes into solution:  $Fe \rightarrow Fe^{2+} + 2e^-$ . Between the points C and D ("passivity" regime), a non-conducting film forms on the iron. This film consists of  $FeCrO_4$  for our chemical components<sup>9</sup>. The so-called "transpassivity" regime, between points D and E is not relevant for the present work. One expects electrochemical oscillations in the vicinity of point C<sup>7,8</sup>. In order to obtain self-oscillations, we slowly increased the voltage  $U$  (see Figs. 2a and 2b) upwards until we reached the passivity regime, i.e. that at which no current  $I$  flows. Then, we carefully changed  $U$  up and down, until we hit the value  $U_c$  (close to C in Fig. 2b) at which autonomous oscillations occur. For the type of setup we used, we found  $U_c$  to be between 1.4V and 1.8V.

The electrode  $Pt_2$  can be removed after oscillations have started. We shall therefore disregard  $Pt_2$  in the rest of this work and we will consider  $U$  to be a measured



**Fig 2.** (a) Scheme of the measuring configuration in the present work. (b) Typical current-voltage characteristic for passivity-activity transitions at a metal-electrolyte interface. (c) Simplified equivalent-circuit scheme of the system without  $Pt_2$ .

or an applied voltage. We shall henceforth describe the system by the simplified equivalent-circuit diagram shown in Fig. 2c. The double layer that forms at the mercury-solution interface<sup>6</sup> is characterized by the capacitor  $C_d$ , the resistance  $R_d$  and the potential  $U_d$ ; the rest of the system is lumped together in the resistance  $R$ .  $I_c$  and  $I_d$  are the currents in the double-layer.  $I_r$  is the current between  $Fe$  and  $Pt_1$ .

Our measured autonomous oscillations are exemplified in Fig. 3a. The observed sharp recurrent peaks are very similar to those in previous reports of oscillations on metal-electrolyte interfaces<sup>8-13</sup>. As one can see in Fig. 3b, which is a blown up small interval of Fig. 3a, our electrochemical oscillations are synchronized with the mechanical oscillations. The latter are described by the radius  $r$  of the drop, which is shown on the same figure and which was determined by hand from video images of the drop on the monitor. We observe a slow increase of  $r$  after the voltage  $U$  drops and a comparatively fast decrease of  $r$  after the rise of  $U$ . Fig. 4 shows the drop, as registered by a video camera from above. Fig. 4a shows circular drops, which are well-centered at the iron, occurring during the first 5-10 min after starting the experiments. Fig. 4b shows distortions occurring later on, as the chemical composition changes (reduction of  $Cr_2O_7^{2-}$  to  $Cr^{3+}$ , as well as dissolution of iron into  $Fe^{2+}$ ; see Ref. 9). Note that the  $Pt_2$  electrode and its support (only needed to get oscillations started) were removed in Fig. 4b. Note also that  $H_2$  is produced by the chemical reaction, accounting for the white spots (bubbles) in Fig. 4. In the present work, we considered only measurements within the first 5 min (circular drop's shape, as in Fig. 4a).

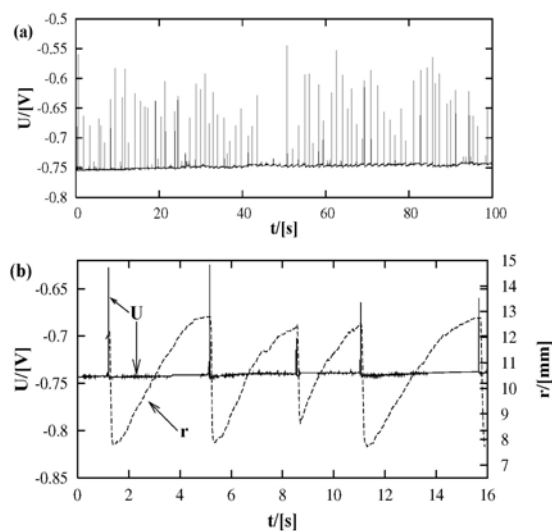


**Fig 3.** (a) Measured oscillations of the potential  $U$ . (b) Enlarged interval of the oscillations of  $U$  (continuous curve) and corresponding oscillations of the drop's radius  $r$  (dashed curve).

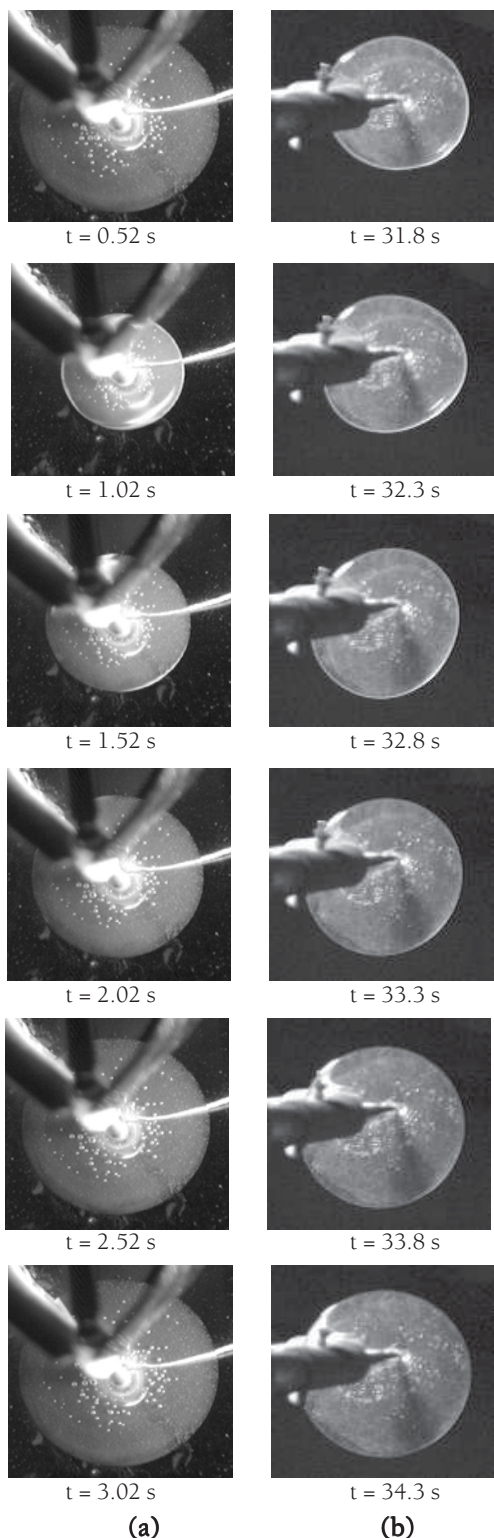


**Fig 4.** Observed oscillations of the drop of oxidizing solution on the mercury surface. (a) Circular, well-centered shapes at times 0.52, 1.02, 1.52, 2.02, 2.52 and 3.02 s. (b) Irregularly swirling shapes after  $\approx 10$  min at times 31.8, 32.3, 32.8, 33.3, 33.8 and 34.3 s.

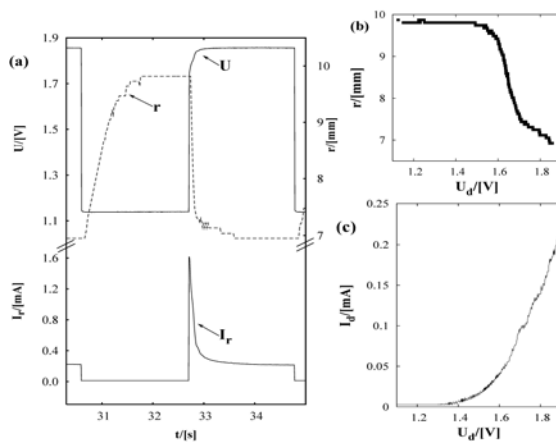


**Fig 5.** (a) Measured responses of the drop's radius  $r$  and the current  $I_r$  to imposed voltage steps of the voltage  $U$ . (b) Measured drop's radius  $r$  vs. the voltage  $U_d$ . (c) Measured current  $I_r \approx I_d$  vs.  $U_d$ .

For a quantitative analysis of the dynamics of the drop, we measured the relaxation of its radius after turning the voltage on and off, as shown in Fig. 5a. For this, we replaced  $Fe$  by  $Pt$  and applied voltages  $U$  (see Fig. 2a);  $Pt_2$  was removed. Comparing Fig. 5a (driven system) and Fig. 3b (autonomous system), we have now a clear indication that, in the self-oscillatory regime, the electrochemical oscillations drive the mechanical oscillations.

Additional data for quantification was obtained by determining the drop's radius  $r$ , as well as the current  $I_d$ , as functions of the voltage  $U_d$  at the double-layer. Note that  $r$  is uniquely defined by  $U_d$  by virtue of the electrocapillarity properties of the drop. Note also that shortly before switching the potential up or down (see Fig. 5a),  $U = U_d$ .  $U_d$  then changes in time, as  $C_d$  is loaded (or unloaded) and approaches a steady state when  $I_c = 0$ .  $r$  follows the temporal changes of  $U_d$ , as shown in Fig. 5a.

In order to measure  $r(U_d)$  and  $I_d(U_d)$ , excluding the relaxation of  $U_d$ , we monitored  $r$  and  $I_d$  by quasistatically increasing  $U$  at a very slow rate, namely 1V/min. (Note that we increased  $U$ , since we had seen in Fig. 5a that the relaxation for upward steps of  $U$  are faster than those for downward steps). The radius of the drop was again determined by hand from video-images on the monitor. We assumed that  $R \ll R_d$  (this will be confirmed by evaluations below), so that the applied potential  $U$  can be set equal to the potential  $U_d$  over the double-layer. The measured dependence of  $r$  on  $U_d$  is shown in Fig. 5b. The steps in Fig. 5b are caused by the limited resolution of our video tool. We found that the evaluation of Fig. 5b at  $U_d > 1.7$  V, at the "shoulder" on the right of the figure, yields results that are not compatible with the rest of this work. Having no

explanation for this “shoulder”, we performed the evaluations leading to Fig. 6b with the restriction  $U_d < 1.7$  V. Fig. 5c shows a typical Butler-Volmer current-voltage dependence<sup>2</sup> with strong shut-off of the current at low voltages.<sup>14</sup>

## EVALUATION OF THE MEASUREMENTS

We call  $\sigma_{SA}$  the surface tension of the solution-air interface,  $\sigma_{MA}$  the surface tension of the mercury-air interface and  $\sigma_{MS}$  the surface tension of the mercury-solution interface. We will do the evaluations using an approximate surface energy analysis. For this we make the rough assumption that the drop has the shape of a flat cylinder with radius  $r$  and height  $h$ . We neglect the surface tension at the electrodes-solution interfaces. We consider that  $\sigma_{SA}$  is given by  $dW/dA$ , where  $W$  is the work done by the system to change the solution-air area  $A = \pi r^2 + 2D/rA$ . The volume  $D$  of the drop is constant. If a change  $dr$  of the radius occurs, the work done by the system is

$$dW = \frac{D^2 \rho}{\pi r^3} g dr + 2\pi(\sigma_{MS} - \sigma_{MA})r dr \quad (1)$$

The first term at the right of Eq. 1 is gravitational work as the height at the center of mass changes by  $dh = -Ddr/\pi r^3$ . The second term is the work done against the force  $2\pi r(\sigma_{MS} - \sigma_{MA})$  at the circular curve shared by air, solution and mercury, at the lower edge of the cylinder. Considering  $dA = 2\pi r dr - 2Ddr/r^2$ , Eq. 1 permits one to determine  $\sigma_{SA} = dW/dA$ . Elimination of  $\sigma_{MS}$  in this last equation then renders

$$\sigma_{MS} = \sigma_{MA} + \sigma_{SA} \left( 1 - \frac{D}{\pi r^3} \right) - \frac{\rho g D^2}{2\pi^2 r^4} \quad (2)$$

$\sigma_{SA} = 70.5$  dyn/cm was given by our measurements with a capillary tube.  $\sigma_{MA} = 471$  dyn/cm is given in the literature and is considered a constant here, assuming that  $\sigma_{MA}$  is unaffected by the electrical charge at the drop. Inserting the measured dependence  $r(U_d)$ , as given by Fig. 5b, in Eq. 2 yielded  $\sigma_{MS}$  as a function of  $U_d$  (electrocapillarity curve), which we show in Fig. 6a. The charge  $q$  per unit area of the double-layer is given by  $q = -d\sigma_{MS}/dU_d$ .  $q$  is shown in Fig. 6b as a function of  $U_d$ , as determined by differentiation of a spline function approximation of the plot shown in Fig. 6a. Such a procedure was also used to differentiate  $q(U_d)$  in Fig. 6b in order to obtain  $C_d = dq/dU_d$ , where  $C_d$  is the differential capacity of the double-layer. The resulting  $C_d$ , as a function of  $U_d$ , is shown in Fig. 6b. An interesting outcome is the fact that the total differential capacity  $dQ/dU_d$ , where  $Q = q\pi r^2$ , can assume negative values. In fact, an increase in  $U_d$  causes a shrinkage of the capacitor's size, which may reduce  $Q$ . More precisely,

$$\frac{dQ}{dU_d} = \pi \frac{d(qr^2)}{dU_d} = \pi r^2 C_d + 2\pi q r \frac{dr}{dU_d} \quad (3)$$

where the second, negative term may dominate over the first. We found this phenomenon for  $U_d > 1.65$  V, for example  $dQ/dU_d = -15 \mu F$  for  $U_d = 1.69$  V.

We now want to comment on the asymmetric changes in  $r$ , as shown in Fig. 5a. Shortly before the voltage  $U$  increases in Fig. 5a, steady state can be assumed.  $U_d = 1.14$  V and Fig. 5c tells us that  $I_d \approx 0$ . This current shut-off at the mercury-solution double-layer remains for a short time after the voltage is increased. Therefore  $I_C \approx I_r$ , i.e. the capacitor  $C_d$  is loaded only with the current passing through  $R$ . A measurement of the sharp decrease of  $r$  with higher temporal resolution than in Fig. 5a ( $r$  is determined by  $U_d$  and is thus an indicator for the loading) yielded a characteristic loading time  $\tau_L \approx 0.04$  s. Considering  $C_d \approx 20 \mu F/cm^2$  (Fig. 6b) and  $r \approx 9.9$  mm (Fig. 5b), we can estimate  $R \approx \tau_L (C_d \pi r^2)^{-1} \approx 650$  Ohm. Comparing  $R$  with the resistances derived from Fig. 5c, we thus confirm  $R \ll R_d$ .

The situation is different for the abrupt decrease of  $U$  in Fig. 5a. Shortly before this decrease, steady state holds. Shortly after the decrease,  $U_d \approx 1.84$  V and  $U \approx 1.14$  V; thus the potential across  $R$  is  $U_r \approx 1.14$  V -  $1.84$  V =  $-0.71$  V. For this voltage, we found that no detectable current  $I$ , flows through  $R$ . (This can also be seen in the left lower part of Fig. 5a). We assume that this current shut-off is related to the double-layer at the Pt-solution interface; such a shut-off has been reported in other works involving Pt.<sup>15,16</sup> Therefore, the capacitor  $C_d$  unloads over  $R_d$ . We can estimate the unloading time  $\tau_U$  considering  $R_d \approx 9.2$  kOhm (Fig. 5c at  $U = 1.84$  V),  $C_d \approx 25 \mu F/cm^2$  (Fig. 6b) and  $r \approx 7$  mm (Fig. 5b at  $U = 1.84$  V). We obtain  $\tau_U = R_d C_d \pi r^2 \approx 0.3$  s, in satisfactory agreement with the measured characteristic time indicated by  $r(t)$  in the upper left of Fig. 5a. It is remarkable that the observed loading-unloading asymmetry holds not only for imposed voltage jumps between Pt electrodes (Fig. 5a), but also for the self-oscillations with the iron needle, which are illustrated in Fig. 3b.

## DISCUSSION

We have observed irregular electrochemical oscillations at an iron-electrolyte system. While both periodical and aperiodical oscillations have been reported in the literature<sup>8-13,17</sup>, we did not obtain periodical oscillations. One reason may be the variations in time of the area of the iron-solution interface in our case; another reason may be a feedback to the iron from the mercury-solution double-layer. It has been

shown before that oscillations of the mercury beating heart can be driven by externally imposed electrical oscillations<sup>18,19</sup>. Analogously, we have driven the system externally (Fig. 5a). We have also shown in our experiments that the mechanical oscillations can be caused by internal self-oscillations (Fig. 3b). Note that while the chemical reactions as well as the electrocapillarity phenomena, are analogous to those of the beating mercury heart, the mechanical oscillator in the present case is not a mercury drop, but a drop of oxidizing solution. The analysis of the mechanical oscillations allowed us to determine the electrocapillarity curve (Fig. 6a), which (excepting the unexplained “shoulder” at the extreme right) has a similar shape as curves reported in the literature<sup>4,6,17</sup>. Also, we could determine the double-layer charge  $q$  and the differential capacity  $C_d$  (Fig. 6b). The values of  $q$  and  $C_d$  are comparable to those reported by Grahame<sup>6</sup> for mercury surfaces in presence of other electrolytes, who reported values of  $C_d$  between 5 and 90  $\mu\text{F}/\text{cm}^2$  and  $|q|$  below 20  $\mu\text{C}/\text{cm}^2$ . Nevertheless, our values may have to be corrected considering that the surface tension could not only be affected by the potential but also by the chemical composition of the double layer (fraction of  $\text{Cr}^{3+}$  in our case).<sup>6</sup>

We want to stress that all voltages appearing in the present work are defined as potential differences between *Pt* and *Pt*, or between *Pt* and *Fe*. This should be kept in mind, when comparing with measurements using standard electrodes, as found in the literature.

A remarkable result of the present work is the existence of a negative capacity. To our knowledge, this is the first experimental observation of a negative d.c. total differential capacity. Finally we want to point out that the beating of the oxidant drop permits one to follow electrochemical oscillations easily with the bare eye, thus being a comfortable visualization method of such oscillations.

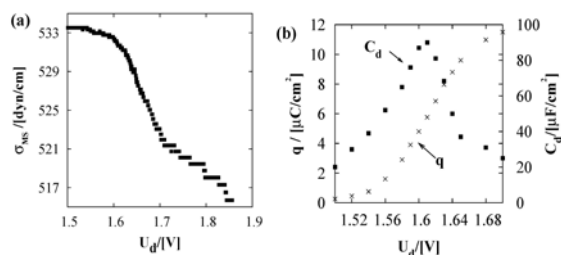


**Fig 6.** (a) Electrocapillarity curve: surface tension  $\sigma_{MS}$  at the mercury-solution interface vs. the potential  $U_d$  over the double layer, as determined from the measurements shown in Fig. 5b. (b) Charge per unit area  $q$  at the drop's bottom, as determined from (a) and differential capacity  $C_d = dq/dU_d$  of the corresponding double-layer.

## REFERENCES

- Lippmann G (1873) Beziehungen zwischen den capillaren und elektrischen Erscheinungen. *Ann Phys Chem* **149**, 547-561.
- Lin S-W, Keizer, J, Rock PA and Stenschke H (1974) On the mechanism of oscillations in the “beating mercury heart”. *Proc Nat Acad Sci USA* **71**, 4477-81.
- Avnir D (1989) Chemically induced pulsations at interfaces: The mercury beating heart. *J Chem Ed* **66**, 211-2.
- Kim CW, Yeo I-H and Paik W-K (1996) Mechanism of the mercury beating heart: an experimental study of the electrochemical-mechanical oscillator. *Electrochimica Acta* **41**, 2829-36.
- Smolin S and Imbihl R (1996) Hydrodynamic modes of the “beating mercury heart” in varying geometries. *J Phys Chem* **100**, 19055-8.
- Grahame DC (1947) The electrical double layer and the theory of electrocapillarity. *Chem Rev* **41**, 441-501.
- Franck UF and Fitzhugh R (1961) Periodische Elektrodenprozesse und ihre Beschreibung durch ein mathematisches Modell. *Z Elektrochemie* **65**, 156-68.
- Sazou D and Pagitsas M (2003) Non-linear dynamics of the passivity breakdown of iron in acidic solutions. *Chaos, Solitons and Fractals* **17**, 505-22.
- Bourceanu G, Melnig V, Vatamanu J and Vasiliu R (1998) Mechanism of electrochemical oscillations in the system  $\text{Fe}/\text{H}_2\text{SO}_4$  (aq),  $\text{K}_2\text{Cr}_2\text{O}_7$  (aq) / Pt. *Electrochimica Acta* **43**, 1031-43.
- Koper M and Sluyters J (1993) A mathematical model for current oscillations at the active-passive transition in metal electrodisolution. *J Electroanal Chem* **347**, 31-48.
- Organ L, Kiss IZ and Hudson JL (2003) Bursting oscillations during metal electrodisolution: experiments and model. *J Phys Chem B* **107**, 6648-59.
- D'Alba F and Lucarini C, (1995) Spontaneous periodic and bursting current oscillations in iron corrosion by dichromate: a useful study for simulating biological systems. *Bioelectrochemistry and Bioenergetics* **38**, 185-189.
- Karantonis A, Shioimi Y and Nakabayashi (2000) Coherence and coupling during oscillatory metal electrodisolution. *J Electroanal Chem* **493**, 57-67.
- Klymenko OV and Compton RG (2004) Mass transport corrected Tafel analysis for electrochemically reversible systems of complex stoichiometry. *J Electroanal. Chem.* **571**, 207-10.
- Pajkossy T and Kolb DM (2001) Double layer capacitance of Pt(III) single crystal electrodes. *Electrochimica Acta* **46**, 3063-71.
- Wu K and Zei MS (1998) Electrochemical behaviour and structural changes of a reconstructed Pt(100) electrode in sulfuric acid: a comparison with Pt(100) - (1X1). *Surface Sci* **415**, 212-26.
- Hudson JL and Tsotsis TT (1994) Electrochemical reaction dynamics: A review. *Chem Eng Sci* **49**, 1493-572.
- Smithwick III RW and Boulet JAM (1992) Electrically driven oscillations of a mercury-droplet electrode. *J Colloid and Surf Sci* **150**, 567-74.
- Olson J, Ursenbach C, Birss VI and Laidlaw WG (1989) Hydrodynamic mode selection due to the electrocapillarity effect: the mercury beating heart in neutral and basic solutions. *J Phys chem* **93**, 8258-63.